ERO2.0 modelling of divertor marker erosion in ASDEX Upgrade L-mode experiments

S. Saari[a,*], A. Hakola[a], J. Karhunen[a], C. Baumann[c], A. Järvinen[a], K. Krieger[b], H. Kumpulainen[c], J. Likonen[a], J. Romazanov[c], ASDEX Upgrade Team[1], EUROfusion Tokamak Exploitation Team[2]

[a] *VTT Technical Research Centre of Finland, Espoo, 02150, Finland*
[b] *Max-Planck-Institut für Plasmaphysik, Garching, 85748, Germany*
[c] *Forschungszentrum Jülich GmbH, Institute of Fusion Energy and Nuclear Waste Management - Plasma Physics, Jülich, 52425, Germany*

Abstract

Erosion of small marker surfaces in an experiment conducted at the ASDEX Upgrade tokamak was modelled using the ERO2.0 code. In the experiment 5×5 mm^2 and 1×1 mm^2 Au marker spots were exposed to a series of high-temperature L-mode plasmas in the low-field side strike point region to serve as proxies for measuring net and gross erosion of W, respectively. An ERO2.0 simulation setup was created for the experiment using background plasma produced using OSM and new angle-dependent reflection and sputtering data for Au generated with the SDTrimSP code. The simulated net erosion of the Au markers agreed closely with the measured values. The erosion of the Au markers was induced mainly by the light B, C and N impurities defined as fixed concentrations in the background plasma. The Au markers were found to undergo up to 15–20 times stronger net erosion in comparison to a uniform W surface. This was attributed to 3–4 times stronger gross erosion of Au in comparison to W and deposition of the eroded Au mostly outside of the markers. Consequently, the simulations suggest strongly compromised capability of Au to act as proxy markers for W in erosion studies due to the significantly higher gross erosion yield of Au and insufficient size of the 5×5 mm^2 markers for successful representation of net erosion, as eroded particles migrate along the plasma flow mostly outside the markers.

Keywords: divertor erosion, ERO2.0, sputtering

1. Introduction

Understanding transport as well as net and gross erosion of tungsten (W) in tokamak-type fusion reactors is crucial in minimizing the harmful effects of high-Z impurities on plasma performance, as well as maximizing the lifetime of the reactor walls. For erosion investigation, it is essential to know the balance between gross and net erosion, i.e., which fraction of the primarily sputtered material is (locally) re-deposited. This can help in the design of plasma pulses to prevent excessive erosion of the plasma-facing components (PFCs), particularly in reactor-scale devices, such as ITER and DEMO.

One way to experimentally study erosion of materials in a tokamak environment is to place carefully designed samples inside the vessel in a desired location and expose them to plasma. Afterwards, net erosion of the samples can be measured experimentally. The first experiments pioneered with this method [1, 2] have been performed in the DIII-D tokamak.

ASDEX Upgrade (AUG) is an excellent environment for studying W erosion in tokamaks [3], as it has been operating entirely with W PFCs since 2007 [4]. It also has an upgraded divertor manipulator (DIM-II) [5], a mechanical system that allows two divertor tiles with samples to be exposed to plasma in the outer strike point (OSP) region with the convenience of removing them from the vessel between plasma discharges.

In this paper, plasma-wall interactions in an experiment [6] conducted at AUG have been modelled using the ERO2.0 [7] and SDTrimSP [8] codes. The simulations are largely based on earlier ERO modelling efforts of the experiment [9], adapting new versions of the modelling tools and an improved simulation setup. The simulation results have not only been compared with experimental results, but the results also aim to examine the validity of the experimental arrangement for studying net and gross erosion of W divertor components with small marker samples, and to consider how the experimental setup could be improved in the future for improved representation of the studied phenomena.

2. Simulation setup

The simulations presented here are based on and compared to the AUG experiment discussed in detail in [6, 9], where net and gross erosion of W were studied around the OSP by exposing gold (Au) marker samples of different sizes to L-mode plasma at different poloidal distances from the strike point. For the experiment, graphite (C) samples of 12×33.5 mm^2, coated with a ~300 nm thick molybdenum (Mo) layer, were equipped with Au marker spots with thickness of ~30 nm. Two markers

*Corresponding author

[1] See author list of "Overview of ASDEX upgrade results in view of ITER and DEMO" by H. Zohm et al., Nuclear Fusion 2024 10.1088/1741-4326/ad249d"

[2] See the author list of "Overview of the EUROfusion Tokamak Exploitation programme in support of ITER and DEMO" by E. Joffrin et al., Nuclear Fusion 2024 10.1088/1741-4326/ad2be4

with a size of 5 × 5 mm^2 or three with a size of 1 × 1 mm^2 were placed along the central line of the samples as presented in figure 1 (a). Three such samples for both marker sizes were placed in a row resulting in 6 larger and 9 smaller Au markers at different distances from the OSP as shown in figure 1 (b).

Au was chosen as a marker material due to its close mass to W and Mo as an intermediate coating because its mass differs significantly from W and Au. Thus, Au on the markers can be distinguished from Mo background using Rutherford Backscattering Spectrometry, which was used after the experiment to determine net erosion rates of the markers.

The marker size of 5 × 5 mm^2 was selected with the intention to represent net erosion based on the expectation of the majority of the eroded Au particles being re-deposited back on the marker surfaces due to the assumed 1–2 mm Larmor radius of Au in the OSP region. By the same rationale, the 1 × 1 mm^2 markers were assumed to showcase gross erosion, as the majority of the particles are deposited outside of the marker surfaces.

The samples were mounted on the target tiles of the DIM-II divertor manipulator and subjected to nine identical L-mode plasma discharges with high electron temperature of $T_{e,OSP}$ = 20–30 eV, resulting in a total plasma exposure time of 28 s. The location of the samples on the AUG divertor in the vicinity of OSP is presented in figure 1 (c).

2.1. Outer target conditions

The applied background plasma for the ERO2.0 simulations is based on OSM [10] simulations aiming at reproducing experimental divertor plasma conditions at the outer target, measured by the Langmuir probes. The outer target electron temperature, T_e, and density, n_e, profiles of the background plasma are presented in figure 2 together with the Langmuir probe data. As there is no measurement data available at the strike point region, due to the lack of a strike point sweep in the experiment, separate simulations were run with manual modifications to the T_e and n_e profiles to address the impact of potential mispredictions by OSM in lack of constraining Langmuir probe data. This included decreasing the peak n_e by ~40% and shallowing the gradient of the T_e profile around the OSP, as shown in figure 2. The ±5 mm uncertainty of the strike point position in the experiment was also tested by shifting the background plasma profiles 5 mm in both poloidal directions. It is emphasized that the modifications and shifting of the background plasma profiles were made only to demonstrate the effect of the uncertainty in the OSP conditions and position with no intention to specifically improve the match to the measured net erosion profiles. The bulk of the analysis is performed using the original background plasma given by OSM.

2.2. Simulation geometry and surface configurations

The simulations were run in a localized rectangular simulation volume of 300 × 300 × 50 mm^3, with 300 × 300 mm^2 toroidal-poloidal wall surface along the outer target, and a volume extending 50 mm perpendicular to the wall surface. The simulation surface configuration with magnifications on regions of interest is presented in figure 3. To replicate the experimental setup, a 300 × 12 mm^2 Mo surface was placed across the toroidal center of the 300 × 300 mm^2 wall surface, on which 5 × 5 mm^2 or alternatively 1 × 1 mm^2 Au markers were positioned with respect to the OSP in correspondence with the experimental arrangement. The 30 nm thick Au markers are elevated 30 nm above the Mo stripe to simulate their thickness. The rest of the simulation surface was defined as W.

The simulation surface was divided into areas of different sizes, such that the areas of interest, i.e., the Au markers and their immediate surroundings 1 mm from their edges — where majority of eroded Au is expected to be deposited — were formed of 0.1 × 0.1 mm^2 surface cells. Since ERO2.0 determines the effect of the background plasma on the surface according to the plasma conditions in the center of each defined

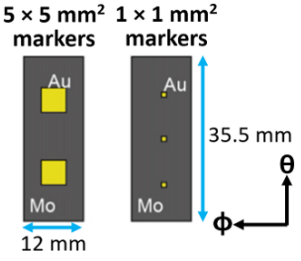

(a) Schematic illustration of the top view of the marker samples. The larger 5 × 5 mm^2 markers were placed approximately 9 mm apart, leaving 7 mm space to the edges of the samples. The smaller 1 × 1 mm^2 markers were placed approximately 7.5 mm apart, leaving approximately 8 mm of space at the ends of the samples.

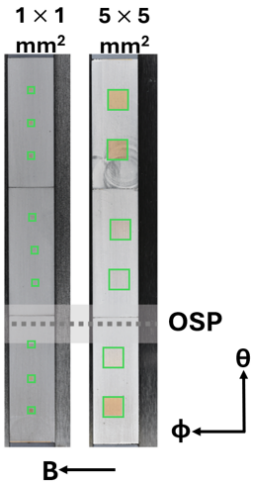

(b) Photo of the test samples. The green squares highlight the positions of the markers on the samples. The dashed line marks the approximative outer strike point position during the experiment.

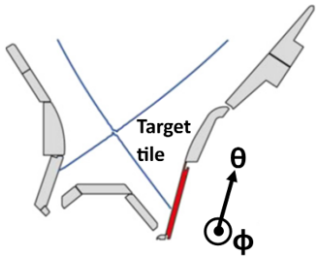

(c) AUG divertor geometry, separatrix (blue lines) and the position of the samples during the experiment (red area).

Figure 1: Samples and their positioning on the LFS divertor target. Figure adapted from [6]. In figure, θ depicts poloidal direction and ϕ toroidal direction.

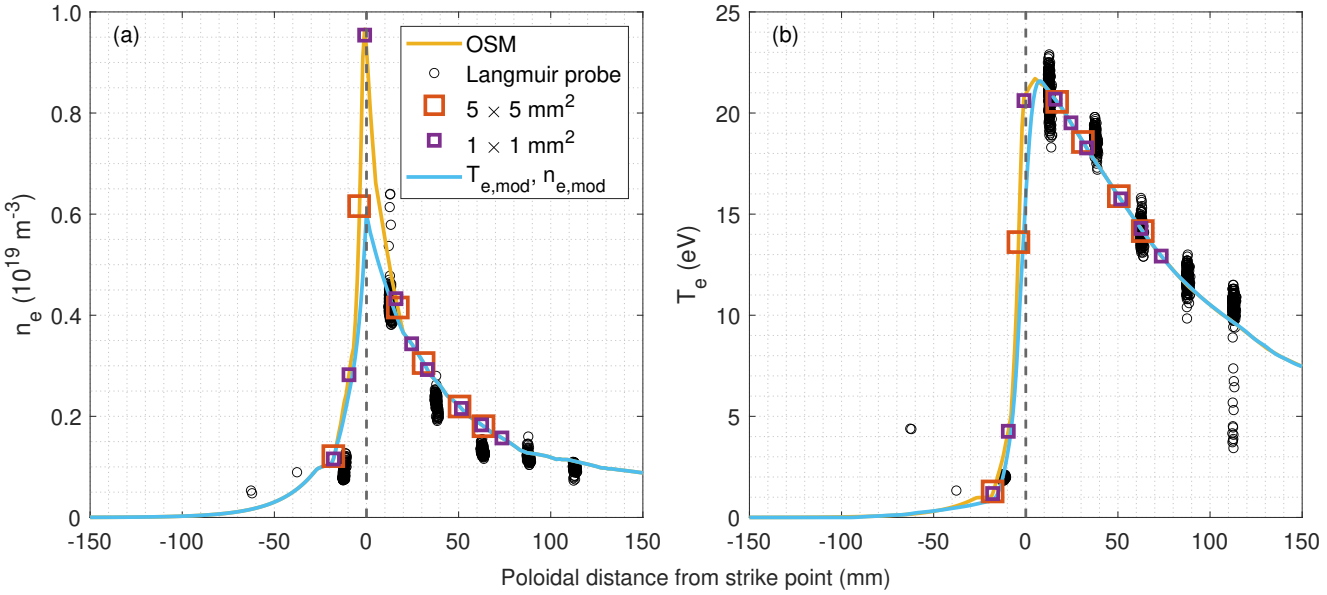

Figure 2: (a) Density and (b) temperature profiles of the background plasma at the LFS target for the OSM plasma and its modifications used in the ERO2.0 simulations. Black circles represent the Langmuir probe data. Larger squares denote the positions of the 5 × 5 mm^2 markers and smaller squares the 1 × 1 mm^2 markers. $T_{\mathrm{e,mod}}$ and $n_{\mathrm{e,mod}}$ represent modified temperature and density profiles of background plasma.

surface cell, dividing into smaller cells increases the spatial resolution of the plasma-wall interaction calculations. Mo located further than 1 mm from the markers was defined as 0.5 × 0.5 mm^2 cells. All the W and rest of the Mo regions over 10 mm from Au markers were divided only poloidally, as their shape had no visible effect on the simulation results.

2.3. Impurities

Fixed concentrations of boron (B), C, nitrogen (N) and W impurities were included in the ERO2.0 background plasma to emulate a typical divertor plasma composition in AUG. Of the impurities, B was chosen because of the regular boronization processes of AUG which together with the N injected during the experiment are intrinsic impurities in the AUG environment. C was assumed to have migrated into the plasma from erosion of the W-coated graphite tiles, and W is always assumed to be present to some extent in the divertor region due to erosion of the first wall. In lack of experimentally determined impurity contents, the applied spatially homogeneous concentrations were $c_{\mathrm{B}} = c_{\mathrm{C}} = c_{\mathrm{N}} = 0.5\%$ and $c_{\mathrm{W}} = 0.05\%$ with respective effective charge states of $Z_{\mathrm{B}} = 3$, $Z_{\mathrm{C}} = 4$, $Z_{\mathrm{N}} = 5$ and $Z_{\mathrm{W}} = 13$, yielding a total effective charge state of $Z_{\mathrm{eff}} = 1.26$. The concentrations and effective charge states of the impurities correspond to those applied in earlier ERO modelling of the experiment [9]. This omits oxygen which is commonly found in AUG plasma but whose omission was found reasonable within the approximative nature of estimating the concentrations and effective charge states of the different impurities. In addition to the fixed impurity concentrations of the background plasma, the Au, Mo and W particles eroded from the surfaces during the simulation were monitored as traced Monte-Carlo test particles with fully tracked migration and ionization.

The sputtering and reflection data between the target and incident particles was primarily obtained from the ERO2.0 database [11], excluding the sputtering and reflection data between Au and other elements which were not readily available. As a major update with respect to the earlier modelling efforts of the experiment [6], the energy- and angle dependent data for Au was produced using the SDTrimSP code as part of this work. The newly generated data replaced the previously used estimates provided by the Bohdansky formula [12] assuming normal incidence without angular dependence. A comparison of sputtering yields of Au bombarded by the different simulation-relevant particle species is demonstrated in figure 4, between yields provided by SDTrimSP at a physically meaningful incident angle of 60° and the Bohdansky formula at normal incidence. The comparison indicates that the yields provided by SDTrimSP are generally higher than those given by the Bohdansky formula by approximately a factor of 5–9, particularly due to the considerations of the incident angle.

3. Results

3.1. Impact of the sputtering data

To study the impact of the new angle-dependent sputtering and reflection data, simulations were run with both the new SDTrimSP data and estimates provided by the Bohdansky formula using the background plasma provided by OSM. Beyond this comparison all results discussed in this work have been obtained using the SDTrimSP data for Au. To minimize statistical noise arising from the small size of the surface cells, the erosion/deposition outputs were averaged in the toroidal direction across the Au markers. Post-processed net erosion/deposition rate profiles for the 5 × 5 mm^2 and 1 × 1 mm^2 Au markers together with the experimental data [6, 9] with its 10–15% (15%

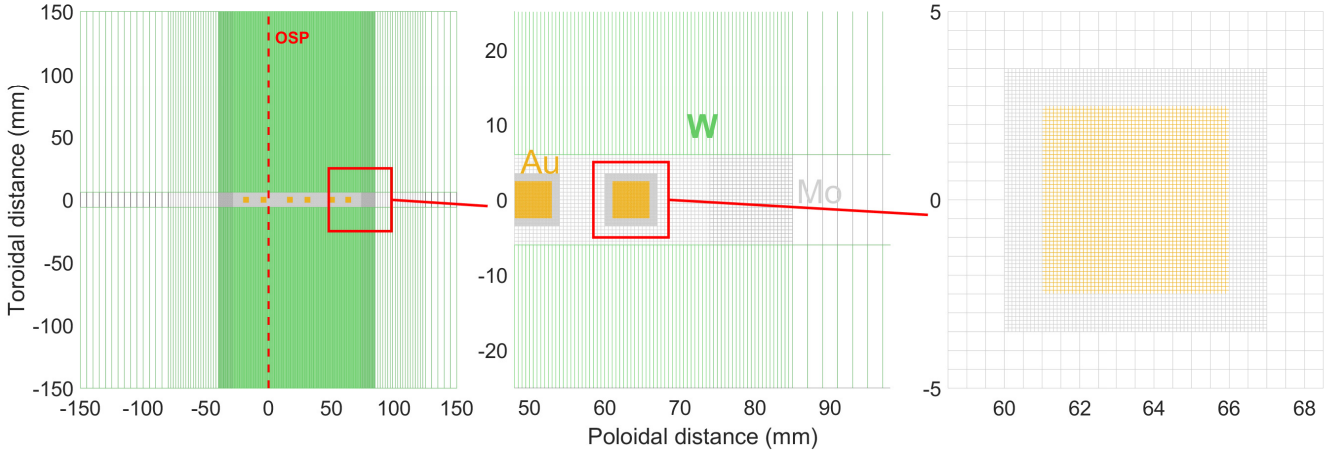

Figure 3: Simulation surface definitions for the 5×5 mm^2 markers with magnification to specific sections pointed by the red squares. W surfaces are presented in green, Mo in grey and Au in yellow. The grid spacing increases when moving towards the edges of the simulation area.

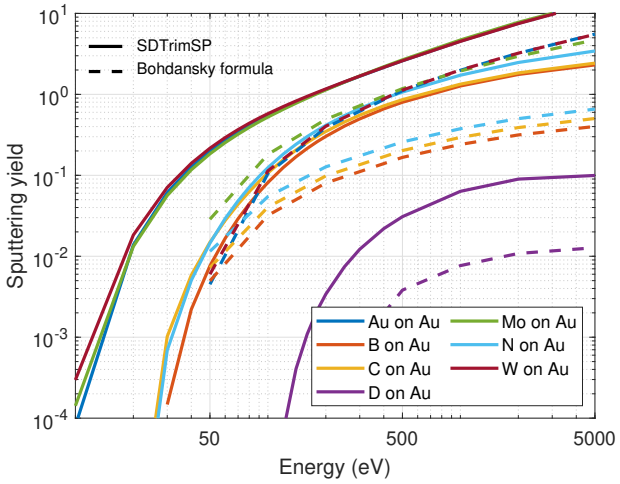

Figure 4: Sputtering yield between simulation-relevant materials and Au as a function of the incident energy. Sputtering yields provided by SDTrimSP (solid line) are presented at a physically meaningful impact angle of 60° and the yields provided by the Bohdansky formula (dashed line) are presented as normal incidence.

used) error margins are presented in figure 5, where negative values denote net erosion and positive values net deposition.

The simulation results obtained using sputtering and reflection data generated with SDTrimSP shows accurate quantitative correspondence to the experimentally measured net erosion rates for the 5×5 mm^2 markers with deviations of less than 30% for the far-SOL markers. In the simulations where the sputtering data is generated using the Bohdansky formula the deviations from the experimental data are 3–4 times larger for each marker, indicating that the new sputtering data has a fundamental role in improving the correspondence of the simulation results to the experimental data. A primary underlying factor is the angular dependence of the SDTrimSP data, which is absent in the Bohdansky formula. The observed increase in net erosion with the introduction of the SDTrimSP data reflects a similar increase in gross erosion of Au in figure 6 where gross erosion and deposition of Au are presented with negative and positive values, respectively. Simultaneously, a similar increase is observed in gross re-deposition of Au on the marker surfaces, such that the ratio of deposition and erosion remained approximately unchanged in the transition from the Bohdansky formula estimates to the SDTrimSP data. This indicates that the increase in net erosion is driven by the higher sputtering yield given by the angle-dependent SDTrimSP data while the newly generated reflection data has a minor effect on the re-deposition of the Au particles.

The agreement of the results with the experimental data for the 1×1 mm^2 markers is not as precise as with 5×5 mm^2 markers, but a good correspondence is obtained especially for the markers located in the near SOL with a similar relative change in net erosion between the simulations runs with the SDTrimSP and the Bohdansky formula sputtering data. At the strike point, the simulations overestimate the measured net erosion of the 1×1 mm^2 markers by approximately a factor of 3. However, this region is characterisized by steep behaviour of the target n_e and T_e profiles, as shown in figure 2, leading to variation of Au erosion by up to an order of magnitude across a narrow range, as observed with the 5×5 mm^2 markers near the OSP in figures 5 and 6. This further motivates assessing the previously discussed remaining experimental uncertainties in the OSP conditions and position when generating the ERO2.0 background plasma, which will be returned to in section 3.2.

3.2. *Re-deposition of eroded Au particles*

The arc-like shape of the net erosion profiles across the markers and the deposition accumulations at the edges of the marker areas observed in figure 5 are due to the spatial dispersion of the eroded Au. In contrast to erosion, deposition is not limited to the marker areas, but Au is also deposited between the markers on the Mo stripe that acts as a substrate, as seen in figure 6. The Au outside the markers in figure 5 primarily originates from the edges of the markers, where the pseudo-random exit angles and momenta of the sputtered atoms drive part of the atoms outside of the marker regions before they are ionised and re-deposited.

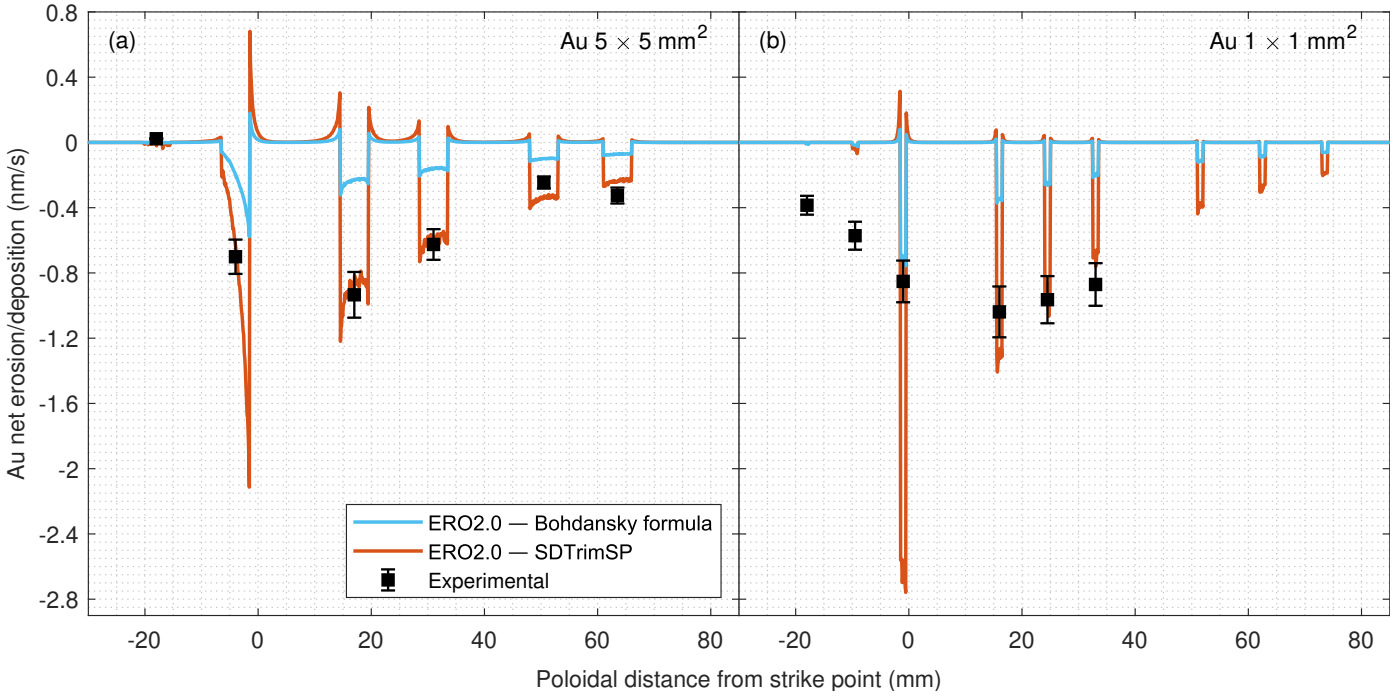

Figure 5: Net erosion/deposition rate profiles for the (a) 5×5 mm^2 and (b) 1×1 mm^2 Au markers obtained with the newly generated SDTrimSP sputtering data (orange) and yield estimates given by the Bohdansky formula (blue). Negative values correspond to net erosion and positive values to net deposition. The black data points with error bars represent the experimentally measured net erosion rates and their 15% uncertainty [6, 9]

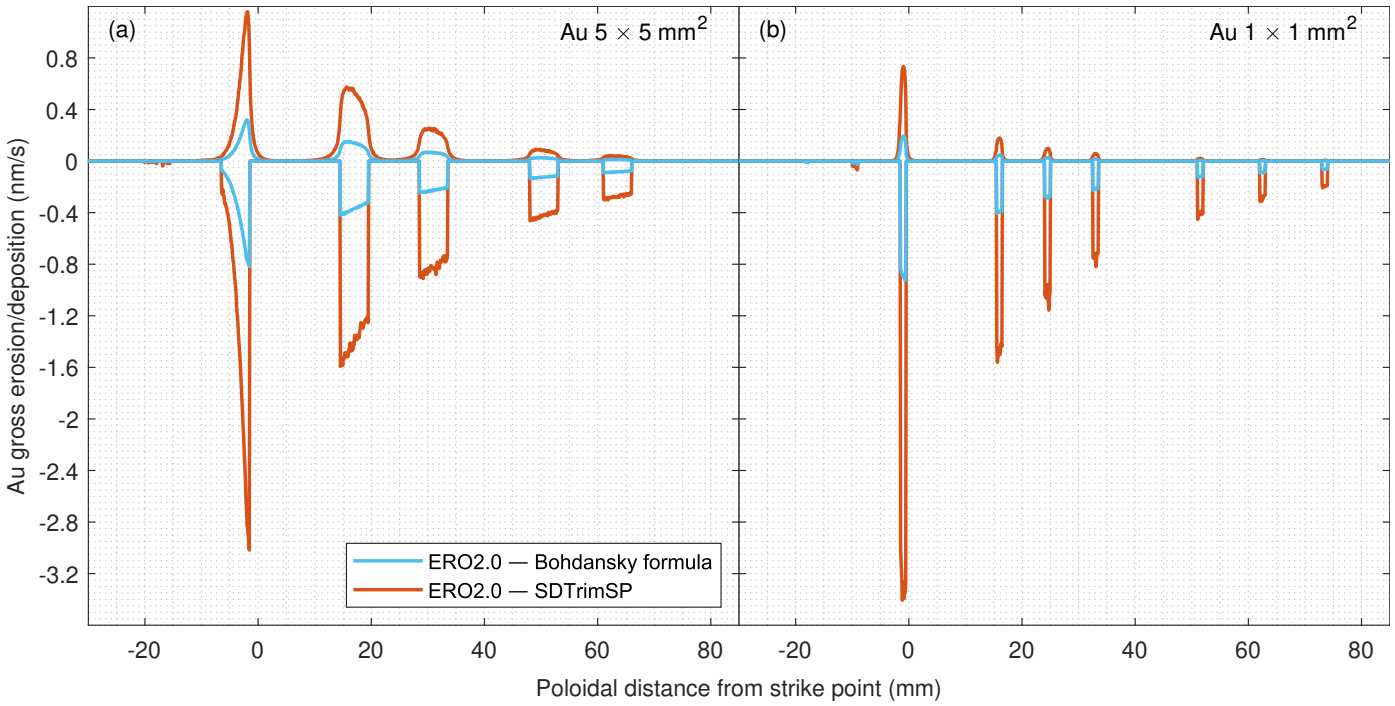

Figure 6: Gross erosion and deposition profiles for the (a) 5×5 mm^2 and (b) 1×1 mm^2 Au markers with sputtering data generated with SDTrimSP (orange) and the Bohdansky formula (blue). Negative values correspond to erosion and positive values to deposition.

To a small extent, the dispersion is also a consequence of particle transport in general, i.e., diffusion and drifts which drive Au particles outside of the marker areas.

The share of the eroded Au particles which re-deposit locally back on the same marker surface decreases with distance from the strike point from approximately 45% and 20% at OSP to 15% and 5% in the far SOL for the 5×5 mm^2 and 1×1 mm^2 markers, respectively. Due to the decrease in the background plasma temperature in the far SOL, the eroded particles are ionized at a lower rate compared to the strike point region and

travel further from the surfaces as atoms before ionizing and migrating back to the target along the plasma flow toroidally downstream from the marker, leading to decreasing local redeposition rate on the markers. It is noted, that the simulations lack the $\vec{E}_r \times \vec{B}$ drift, due to the inability of ERO2.0 to consider the radial electric field, $\vec{E}r$, in the applied Cartesian coordinate system at the time of carrying out the work. At the target, this would drive ions towards the wall surface, thereby potentially returning more sputtered particles closer to their original erosion site.

Due to the dominance of entrainment with the parallel plasma flow over other transport phenomena, the migration of the eroded Au particles occurs mainly in the toroidal direction downstream from the markers, as can be seen in figure 7, which shows the deposition of particles eroded from the 5×5 mm^2 markers on the simulation surface. The figure also shows that the deposition flux is poloidally inclined towards the OSP, which indicates a role of the radial $\vec{E}_\theta \times \vec{B}$ drift. However, the plot mainly depicts the migration of particles along the plasma flow in a positive toroidal direction.

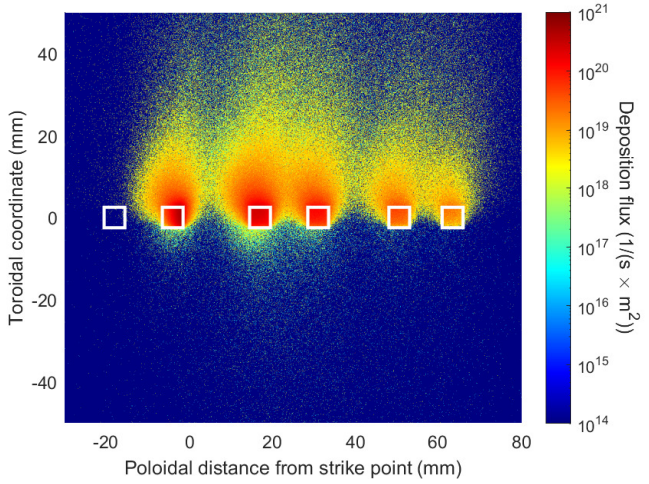

Figure 7: Deposition flux of Au eroded from the 5×5 mm^2 Au markers. The plasma flow is directed towards the positive toroidal coordinates. The white squares represent the 5×5 mm^2 Au marker positions. Note the logarithmic colour scale.

3.3. Assessment of the uncertainty of the outer strike point position and conditions

The experimental uncertainty of the strike point position and its effect on the simulations has been tested by shifting the background plasma 5 mm in both negative and positive poloidal directions. As shown in figure 8, with the larger 5×5 mm^2 markers the match to the experimental data does not significantly improve for any marker in comparison to the already good match obtained with the original strike point position but rather degrades it near the strike point position. However, a shift in the negative poloidal direction with the 1×1 mm^2 markers improves correspondence with the experimental data especially for the markers around the strike point, which highlights the fact that the inability to experimentally pinpoint the exact strike point position can have a noticeable effect on the accuracy of the simulations against the experimental data. However, the OSP shifts cannot fully explain the remaining discrepancies between the simulated and measured erosion rates.

Applying modifications to the target n_e and T_e profiles around the OSP within the freedom allowed by the missing Langmuir prode data as discussed in section 2.1, is demonstrated to have notable effects on the simulated net erosion in figure 9. The selected demonstrations of decreasing the peak n_e by ~40% and reducing the T_e gradient near the OSP were applied both individually and in combination to assess their collective impact, which were observed to significantly decrease simulated net erosion of the marker nearest to the OSP. In the case of the 1×1 mm^2 markers, this noticeably reduces the overestimation of the OSP erosion in comparison to the experimental measurements. To reduce the degrees of freedom originating from the uncertainties, it is thus found essential to perform a strike point sweep during the experiment to provide continuous n_e and T_e profiles at the outer target and, consequently, improved constraints for the generating of the background plasma for the simulations.

3.4. Assessment of Au markers as proxy for erosion of W PFCs

The representativeness of the localized Au markers in relation to the more uniform divertor W wall of the tokamak was also tested by considering a pair of hypothetical simulation setups, where all the surface materials of the original configuration were changed fully to Au and then W respectively. The net erosion/deposition curves obtained these simulations were then compared to the simulation results obtained with the markers (figure 5). Taking into account that the background plasma is toroidally symmetric, the all-Au and all-W erosion curves were taken from the toroidally extended surfaces — defined as W in figure 3 — for balanced representation of erosion and deposition without significant impact of migration of the eroded material in the toroidal direction along with the parallel plasma flow. Since W is present in the simulations both as traced particles eroded from the simulation surface and a constant concentration in the background plasma, the net erosion curve of W was also calculated such that the W deposition from the background plasma was not taken into account. While this reduces the physical meaningfulness and experimental relevance of the analysis, it provides a parallel case with improved comparability to the net erosion of Au, as Au has no fixed presence in the background plasma of the simulations. Since the larger 5×5 mm^2 markers were intended for net erosion studies, they have been compared to the net erosion curves of the toroidally extended surfaces, while the smaller 1×1 mm^2 markers, intended for gross erosion studies, have been compared to the gross erosion curves of the Au and W surfaces.

Net erosion of the 5×5 mm^2 Au markers is observed to be 2–6 times stronger compared to the toroidally extended Au surfaces. The main reason is that, unlike in the case of the toroidally localised markers, most of the Au eroded from the large surfaces is deposited back onto the same surface. This can be seen in figure 11 (a) which shows that, although gross

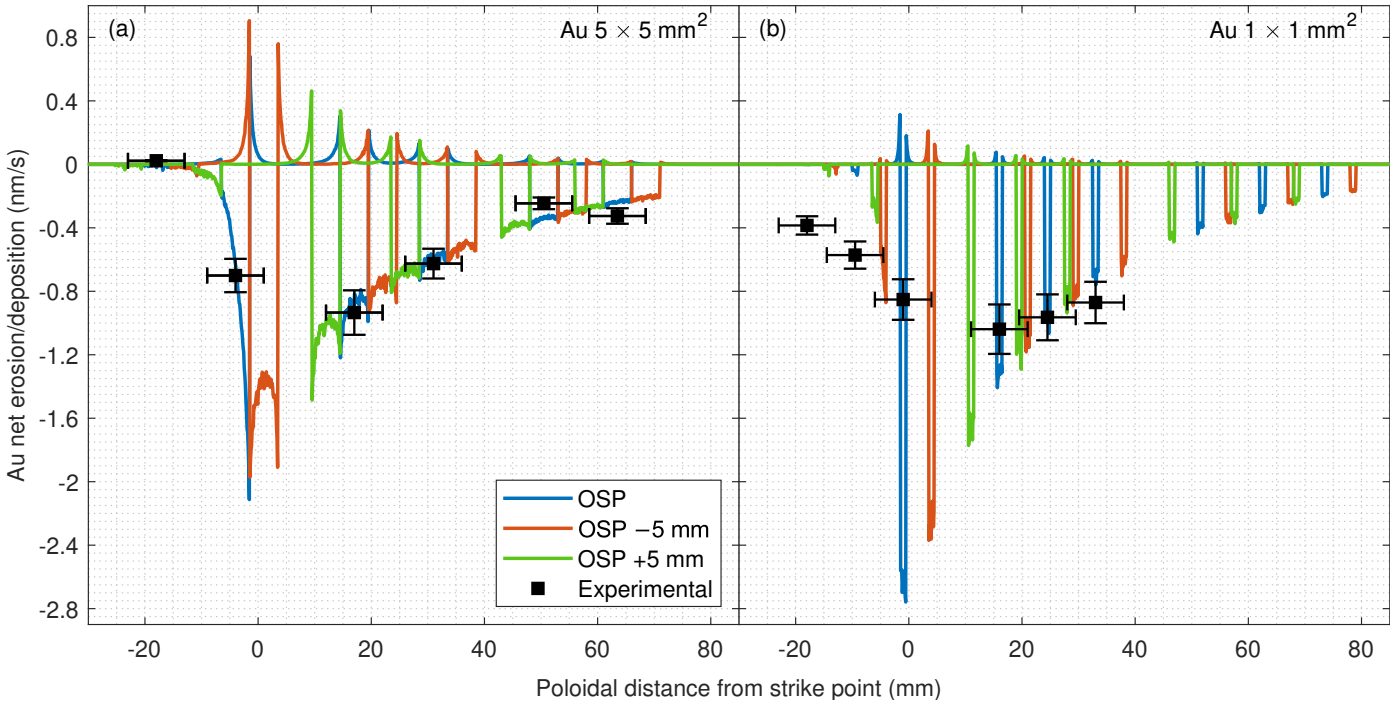

Figure 8: Net erosion/deposition profiles for the (a) 5×5 mm^2 and (b) 1×1 mm^2 Au markers plasma with shifted strike point positions. The background plasma is moved 5 mm in negative (red) and positive (green) toroidal directions. Negative values correspond to net erosion and positive values to net deposition. 5 mm horizontal error bars depicts the uncertainty of the strike point position and 15% vertical error bars depicts the uncertainty of the experimental data.

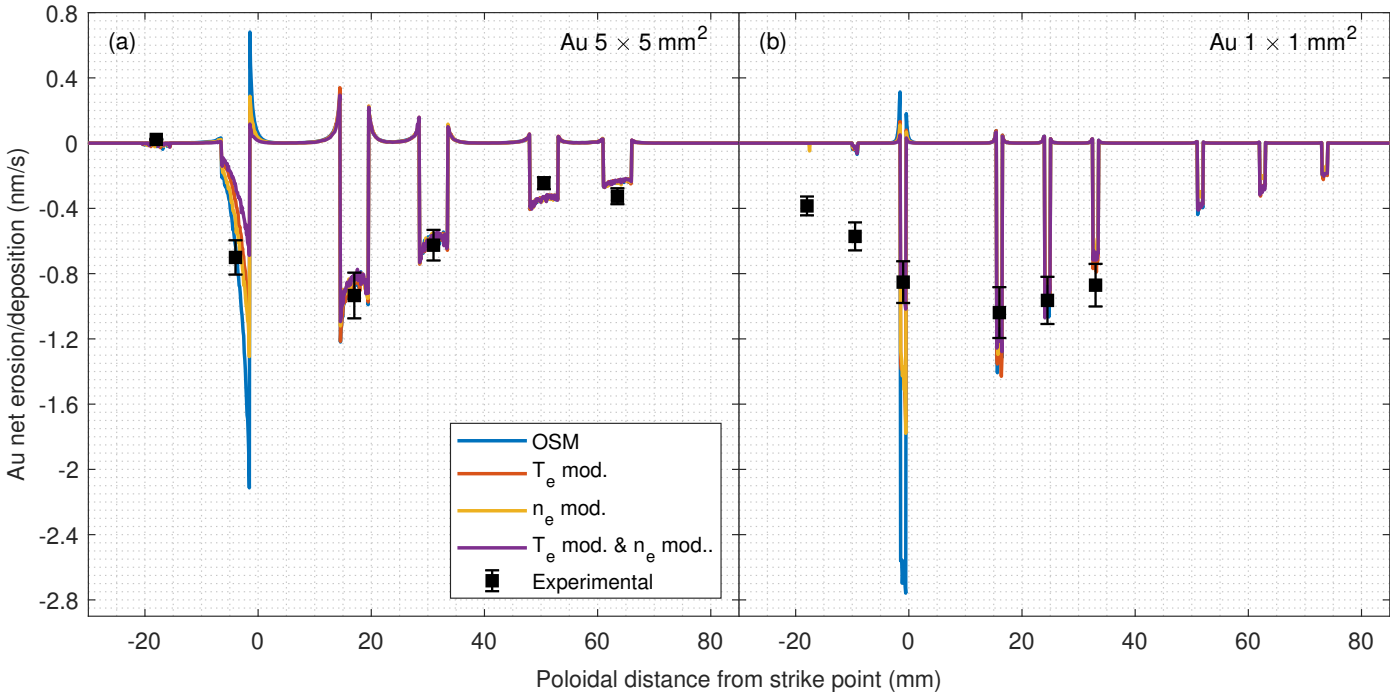

Figure 9: Net erosion/deposition profiles for the (a) 5×5 mm^2 and (b) 1×1 mm^2 Au markers obtained by using modified background plasma density and temperature profiles in the OSP region. Negative values correspond to net erosion and positive values to net deposition. The black squares with error bars represent the experimentally measured net erosion rates with 15% uncertainty.

erosion of the large Au surfaces is identical to that of the markers, deposition on them is 2–3 times stronger compared to the deposition on the Au markers. Hence, it can be concluded that the 5×5 mm^2 markers are too small in the toroidal direction for net erosion studies due to excessive share of the eroded Au migrating beyond the marker areas before re-deposition as shown in figure 7. In contrast, for the 1×1 mm^2 markers, where gross deposition is low, the net erosion curve of the markers

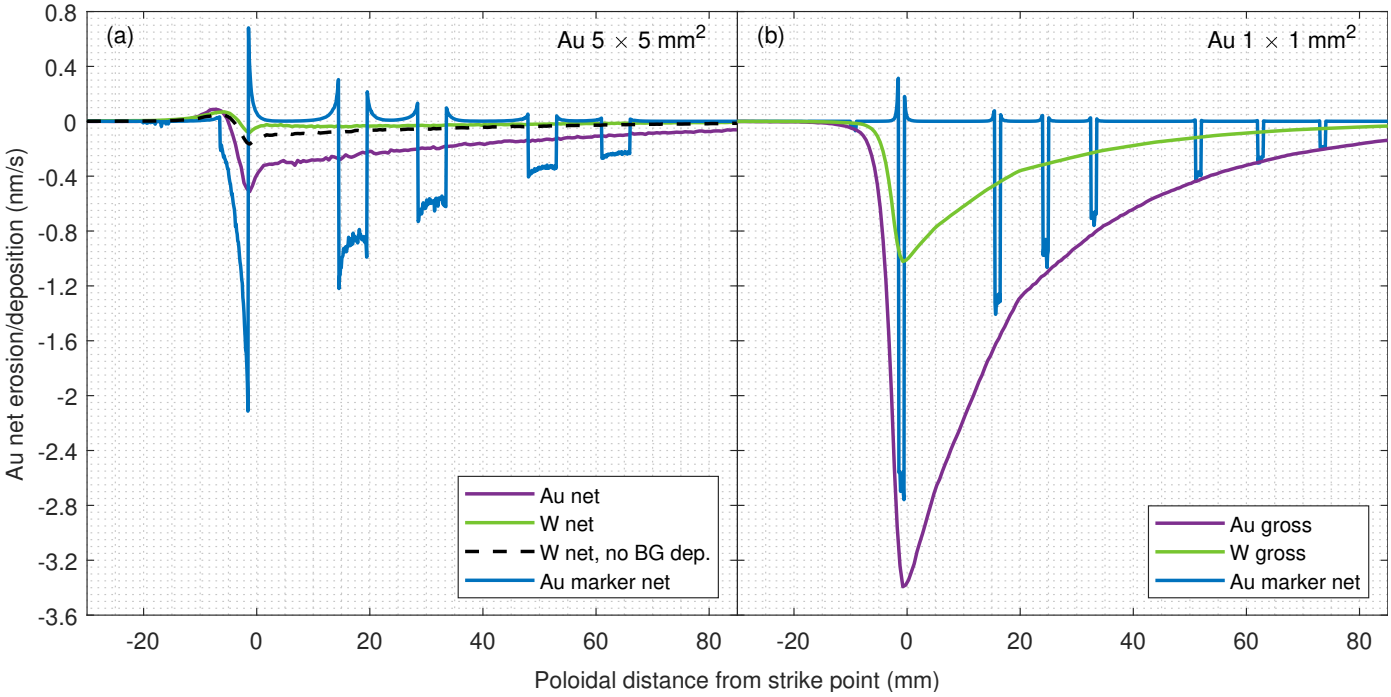

Figure 10: Net erosion profile of the all-W — with and without deposition from the background plasma — and all-Au surface configurations together with the 5 × 5 mm^2 Au markers (a) and gross erosion profiles of all-W and all-Au surface configurations along with the net erosion rates of the 1 × 1 mm^2 Au markers (b). Negative values correspond to net erosion and positive values to net deposition.

agrees with the gross erosion curve of the toroidally extended Au within 20% in figure 10 (b), suggesting that the 1 × 1 mm^2 marker geometry is fairly suitable for gross erosion studies.

Comparison between the toroidally extended Au and W surfaces shows approximately a factor of 6 higher net erosion of the former in figure 10 (a) — reducing to a factor of 3, if deposition of W from the background plasma is omitted — resulting from the 3–4 times higher gross erosion rate of Au observed in figures 10 (b) and 11. This implies that Au is quantitatively a suboptimal proxy for studying W erosion, and other materials, such as platinum, should be considered in future studies. Combining geometry and material effects, the 5 × 5 mm^2 markers end up overestimating net erosion of the toroidally continuous W surfaces by a factor of 15–20, while gross erosion of W is overestimated by a factor of 3–4 by the 1 × 1 mm^2 markers.

3.5. Role of different impurity species

Figure 12 shows the contribution of different ion species to gross erosion of the Au markers in the simulations. Erosion can be observed to be mainly dominated by light impurity ion species, i.e., B, C and N. These three particle species each had the same concentration in the background plasma but different effective charge states. N, the heaviest element of these with the highest effective charge state, has the largest contribution to the gross erosion, covering 30–35% of it per marker. B, on the other hand, being the lightest with the lowest effective charge state, accounts for only 13–15% of gross erosion per marker. However, it is worth noting that since there is no measurement data of the composition of the plasma during the experiment, the impurity concentrations in the ERO2.0 background plasma are a rough but justified estimate of the actual composition. Different variations of the background plasma will be tested in the future. The low charge state and mass of deuterium (D) lead to negligible erosion of Au, even at the markers closest to the strike point. According to the newly generated SDTrimSP sputtering data, the sputtering threshold energy for Au under D bombardment at 60° incidence is of the order of 100 eV, which is exceeded only at the OSP with the peak outer target electron temperature of 22 eV in the simulations.

Au self-sputtering is negligible under the present conditions, although its self-sputtering yield according to the SDTrimSP simulations is comparable to that of the sputtering yield caused by W as seen in figure 4. This can be explained by the fact that the eroded Au returns to the markers mainly locally as low-energy particles that do not exceed the sputtering threshold energy. However, self-erosion of Au is somewhat noticeable on the 5 × 5 mm^2 markers nearest to the strike point, where the background plasma temperature is at its highest. Considering the rather small amount of W introduced in the simulations, the erosion caused by it is fairly strong per marker. The main part of the W-induced erosion arises specifically from the background plasma, which acts toroidally symmetrically across the simulation surface. In contrast, eroded W, which is traced as test particles, plays a minor role since it originates far from the markers. In addition, the ionization state of the eroded W, Mo and Au particles returning to the wall surface is small compared to the effective charge state, $Z_W = 13$, set for W in the background plasma.

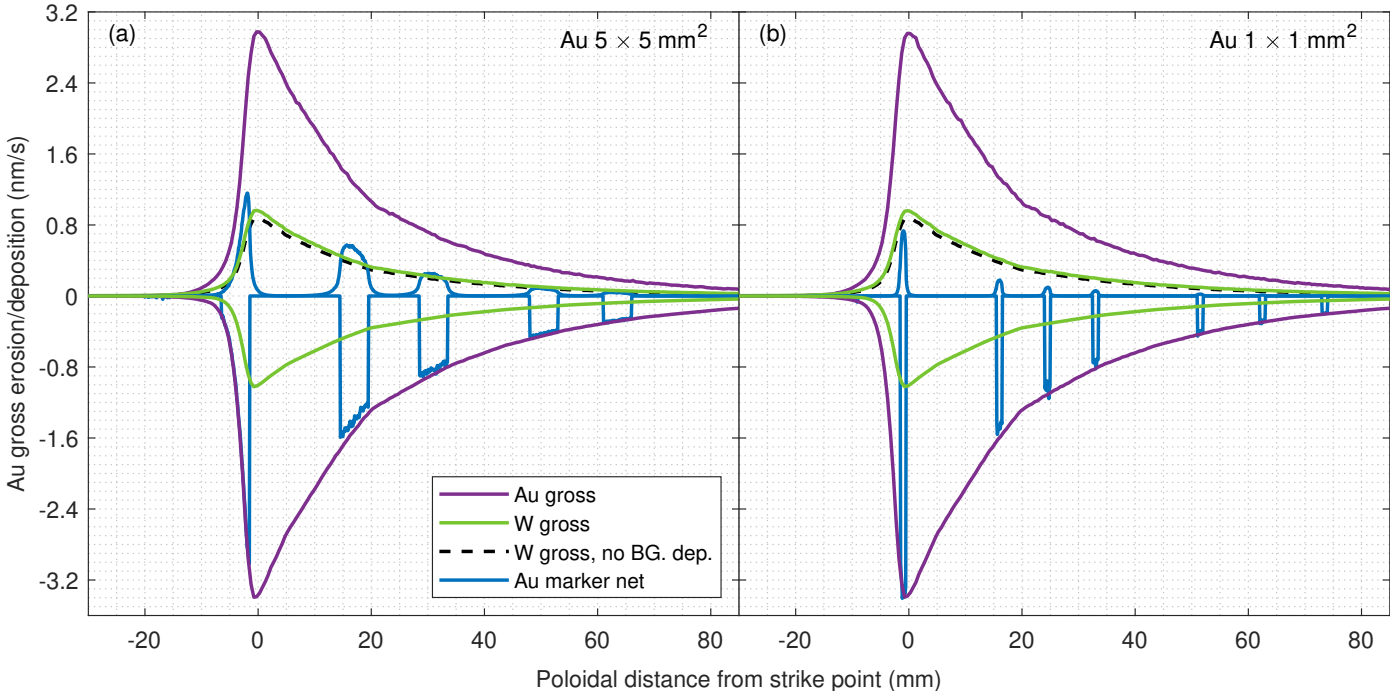

Figure 11: Gross erosion and deposition profiles for the toroidally extended W and Au surfaces together with the (a) 5×5 mm^2 and (b) 1×1 mm^2 Au markers. Negative values correspond to gross erosion and positive values to gross deposition.

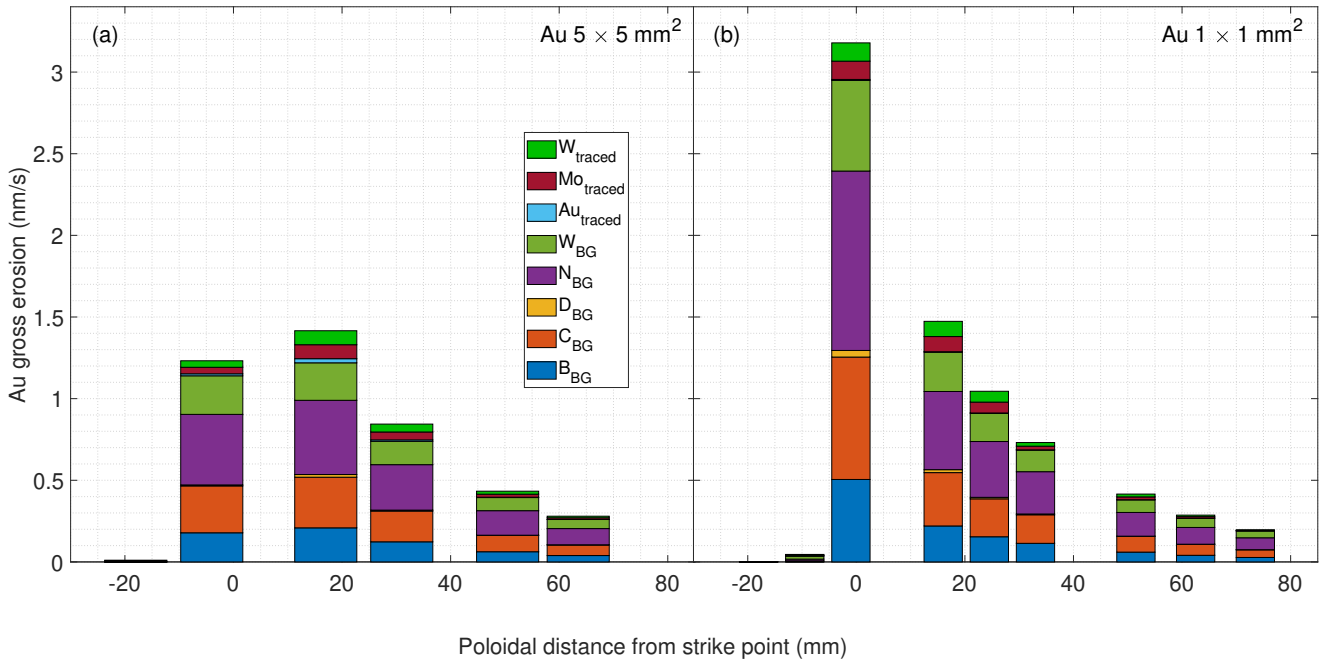

Figure 12: Contributions of the different particle species in gross erosion of the (a) 5×5 mm^2 and (b) 1×1 mm^2 Au markers.

4. Discussion and Conclusions

This paper discusses ERO2.0 modelling of an AUG experiment, where Au markers were exposed to L-mode plasma discharges in the OSP region as proxies for studying erosion of the W components. New sputtering and reflection data were generated for Au using the SDTrimSP code for improved representation of the erosion of the markers under bombardment by D and various impurity species included in the simulations.

The simulation results show primarily good agreement within less than 30% with the experimentally measured erosion rates of Au, especially for 5×5 mm^2 markers, aiming at net erosion studies, but also for smaller 1×1 mm^2 markers,

providing adequate information of gross erosion, albeit with larger discrepancies remaining for the latter at the OSP and in the PFR.

The single biggest factor in improving the correspondence to experimental results with respect to earlier ERO modelling of the experiment was the new sputtering and reflection data produced with SDTrimSP, which, especially due to the angle dependence, significantly increased the erosion yield of Au from the previously applied estimates given by the Bohdansky formula with no angular dependence. The simulated erosion profiles of Au were found to be prone to uncertainties in preparation of the background plasma for ERO2.0, arising from lack of Langmuir probe data for n_e and T_e of the strike point.

The study also found the larger 5×5 mm^2 markers not suitable for net erosion studies due to their insufficient size in the toroidal direction. Most of the particles eroded from the Au surfaces are migrated toroidally away from the markers by the parallel plasma flow, and re-deposition of Au back on the marker surfaces was strongly underestimated with respect to toroidally extended Au surfaces. However, on the 1×1 mm^2 markers the simulated net and gross erosion rates in the PFR agreed within 20% indicating that the small markers work relatively well in gross erosion studies. Large discrepancy near the strike point is most likely due to the inaccuracy of its position.

In the simulations, erosion of the Au markers was caused especially by the light impurities of the background plasma: B, C and N each of which having a crudely estimated fixed concentration of 0.5% in the divertor plasma. The contribution of W, particularly as a fixed 0.05% concentration in the background plasma, was also found significant in the gross erosion of Au. The fully traced eroded Au, Mo and W particles were found to have a far lesser impact on the erosion of the markers, as they mostly return to the surface with low energies and low ionisation states. The findings of this work suggest that in future erosion experiments an alternative proxy material that more closely resembles W erosion should be used instead of Au. for improved representation of the erosion of the W wall. Also, the use of toroidally extended proxy material surfaces could improve net erosion studies, allowing a larger proportion of the eroded particles to return to the surface under study.

Acknowledgements

This work has been carried out within the framework of the EUROfusion Consortium, funded by the European Union via the Euratom Research and Training Programme (Grant Agreement No 101052200 — EUROfusion). Views and opinions expressed are however those of the author(s) only and do not necessarily reflect those of the European Union or the European Commission. Neither the European Union nor the European Commission can be held responsible for them.

References

[1] P. Stangeby, et al., J. Nucl. Mater. 438 (2013).
[2] J. Guterl, et al., Plasma Phys. Control. Fusion 61 (2019) 125015.
[3] H. Meyer, et al., Nucl. Fusion 59 (2019) 112014.
[4] R. Neu, et al., Nucl. Mater. Energy 438 (2013).
[5] A. Herrmann, et al., Fusion Eng. Des. 98-99 (2015) 1496.
[6] A. Hakola, et al., Nucl. Fusion 61 (11) (2021) 116006.
[7] J. Romazanov, et al., Phys. Scr. (2017) 014018.
[8] A. Mutzke and others, SDTrimSP Version 6.00, IPP Report (2019).
[9] A. Hakola, et al., Nucl. Mater. Energy 25 (2020) 100863.
[10] P. Stangeby, et al., Nucl. Fusion 35 (1995) 1391.
[11] ERO data project repository, https://jugit.fz-juelich.de/ero/amns (2025).
[12] J. Bohdansky, et al., Nucl. Instr. and Meth. B 2 (1984) 587.